Chapter 3

Azidation of Silicon(111) Surfaces

The contents presented in this chapter are based on Cao, P.G., Xu, K. and Heath, J.R. "Azidation of silicon(111) surfaces," *J Am Chem Soc*, 130, 14910-14911 (2008). (Ref.[1])

3.1 Introduction

The passivation of nonoxidized silicon surfaces has emerged as a potential method for protecting the silicon surface from oxidation,[2-8] for improving the electronic properties of ultrathin silicon films,[9, 10] and for adding new chemical function to those surfaces.[11-19] The Si(111) surface has provided the template for much of this chemistry. In Chapter 1, we have systematically studied the morphology and surface electronic structures modified through capping silicon atop sites with chlorine atoms. While the atop sites on the unreconstructed Si(111) surface may be fully passivated with H, Cl or Br atoms, those surfaces are unstable to oxidation.[20, 21]

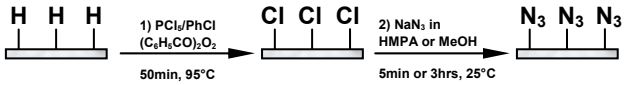

Figure 3.1. A schematic showing the two-step chlorination/azidation surface synthetic process.

Full passivation (close to100%) of the silicon atop sites with methyl[22] or acetyl[23] groups has also been achieved. Those surfaces (H_3C-/Si(111) and HC≡C-/Si(111)) are

stable against oxidation, which is reflective of both the high coverage and the stability of the Si-C bond. In this chapter, we report on a two-step chlorination/azidation process (Figure 3.1) for the chemical passivation of Si(111) surfaces with azide groups, and we report on the detailed chemical and structural characterization of those surfaces.

3.2 Experimental

3.2.1 Materials and methods

Anhydrous inhibitor-free tetrahydrofuran (THF, ≥99.9%, water content <0.002%), anhydrous methanol (99.8%, water content <0.002%) and hexamethylphosphoramide (HMPA, 99%) was purchased from Sigma-Aldrich. Prior to use, HMPA is dried with calcium hydride (reagent grade, 90-95%, Sigma Aldrich) overnight. Phosphorus pentachloride (PCl_5, 99.998%) was purchased from Alfa Aesar. These reagents were used as supplied and stored in a glovebox purged with nitrogen. Silicon samples were (111)-oriented, Sb-doped, n-type Si wafers with a low miscut angle of ±0.5° and a resistivity of 0.005-0.02 ohm·cm. Samples were obtained from ITME (Poland).

Silicon wafer was cut into samples of 0.5×1 cm pieces. The crystal orientation was marked according to the flat along the side of the wafer. The silicon wafers were first sonicated in acetone and methanol for 5 min each followed by a standard RCA cleaning process. The samples were then immersed in degassed 40% NH_4F for 15 min to prepare atomically flat H-/Si(111). Chlorination was performed by treating H-/Si with PCl_5 in chlorobenzene at 95^{o}C for 50 min in a nitrogen-purged glovebox. The Cl-/Si(111) surfaces were then rinsed with tetrahydrofuran (THF) and methanol and exposed at 25^{o}C under inert atmosphere to solutions of sodium azide (NaN_3, ≥99.5%, Sigma Aldrich) in

either HMPA or methanol for 5 min and 3 hrs, respectively. Following the reaction, the sample was removed from the solution and rinsed thoroughly with THF and methanol. After 5-10 min sonication in methanol, the sample was dried under streaming N_2(g).

3.2.2 Instrumentation

X-ray Photoelectron Spectroscopy: All spectra were collected in a UHV vacuum chamber maintained at a pressure of $<1.0\times10^{-9}$ Torr using an M-Probe XPS system that has been described elsewhere.[24] Monochromatic Al Kα source radiation (1486.6 eV) was incident near the middle of the sample at an angle of 35° off the surface. Photoelectrons emitted along a takeoff angle of 35° from the surface were collected by a hemispherical analyzer. The ESCA software (version 102.04, Service Physics, Inc.) available with the instrument was used for both data collection and analysis.

Infrared Spectroscopy Measurements: A Vertex 70 Fourier transform infrared (FT-IR) spectrometer (Bruker Optics, Inc.) was used to collect the attenuated total reflection infrared (ATR-IR) data of the sample. The sample was mounted on a germanium ATR crystal (*G*ATR, Harric Scientific Products, Inc.) with a grazing angle of 65°. The sample compartment was purged with dry and CO_2-eliminated air for ~5 min before each background/sample data collection.

Scanning Tunneling Microscopy and Scanning Tunneling Spectroscopy: The topographic and spectroscopic data were collected on an Omicron low-temperature UHV STM system using mechanically cut Pt/Ir tips. The vacuum pressure was maintained at $<10^{-10}$ Torr. Detailed description can be found in Chapter 2.

3.2.3 Surface coverage calculations

The surface coverage of species was estimated by referencing all peaks to the Si 2p peak at 99.4 binding eV (BeV). For multi-overlayers on the Si(111) surface, a substrate-overlayer model can be used to obtain the fractional monolayer coverage. Assuming negligible difference in the escape depths for photoelectrons excited from overlayer and substrate orbitals (i.e., λ_{ov} (ovBE) ≈ λ_{ov} (sbBE) = λ_{ov}), the overlayer thickness, d_{ov}, was obtained,[25, 26]

$$d_{ov} = \ln[\left(\frac{I_{ov}}{I_{Si}}\right)\left(\frac{SF_{Si}}{SF_{ov}}\right)\left(\frac{\rho_{Si}}{\rho_{ov}}\right)+1]\lambda_{ov}\mathrm{Sin}\theta \qquad (3.1)$$

where θ is the takeoff angle (θ =35°), ρ_x and I_x are the volumetric density and integrated area of the signal of the overlayer and Si, as indicated, and SF_{Si} and SF_{ov} are the modified sensitivity factors for the Si 2p peak and the chosen overlayer peak, respectively. Here, $SF_{Si\ 2p}$=0.90, $SF_{C\ 1s}$=1.00, $SF_{O\ 1s}$=2.52, $SF_{Cl\ 2p}$=2.40 and $SF_{N\ 1s}$=1.80. The overlayer thickness was then divided by the monolayer thickness to estimate the fractional monolayer coverage.

For submonolayer (i.e., the fractional monolayer coverage Φ_{ov}<1), an alternative formulation would be[5, 6]

$$\Phi_{ov} = \left(\frac{\lambda_{ov}\mathrm{Sin}\theta}{a_{ov}}\right)\left(\frac{SF_{Si}}{SF_{ov}}\right)\left(\frac{\rho_{Si}}{\rho_{ov}}\right)\left(\frac{I_{ov}}{I_{Si}}\right) \qquad (3.2)$$

where a_{ov} is the atomic diameter of the species in the overlayer.

Azide: Assuming that 100% coverage of azides on Si(111) is obtained when every atop Si(111) atom is capped by one azide molecule, then the formulation (3.2) for sub-monolayer would be appropriate for the azide coverage calculation, since it is likely Φ_{azide}<1. Furthermore, $a_{ov}\rho_{ov}$ can be substituted by $3n_{Si,surf}$ since one azide moiety

contains three nitrogen atoms. Here, $n_{Si,surf}$ is the surface number density of Si atoms (7.8×10^{14} atoms cm^{-3} for Si(111)). The escape depth through the azide layer can be approximated using the empirical equation[25] $\lambda_{ov} = 0.41a^{1.5}E^{0.5}$, where E (in eV) is the electron kinetic energy and a is the diameter of the atoms in the monolayer. The attenuation factor for Si 2p and N 1s electrons through the azide monolayer was then calculated to be 2.5 and 2.2 nm, respectively. The former value was used to simplify the calculations.

Chlorine: Similar to the azide case, Equation (3.2) was used for coverage calculations. Here, $a_{ov}\rho_{ov} = n_{Si,surf}$ and $\lambda_{ov} = 2.6$ nm for the Si 2p electrons.[25]

Carbon: The assumption of 100% coverage is slightly different from the above azide and chlorine cases. The overlayer was assumed to consist of carbon atoms packed with a solid-state volumetric density (ρ_{ov} = 1.51×10^{23} atoms cm^{-3}) and to have a monolayer thickness equal to the atomic diameter of carbon in its solid state ($a_{ov} = 0.19$ nm). This definition is for convenient comparison with that in the literature. Here, the escape depth for the Si 2p electron was calculated to be 1.3 nm. Then the use of the coverage calculation method would depend on the fractional coverage value.

Oxygen: Similar to carbon above, the use of the coverage calculation method also depends on the fractional value. Here, $\lambda_{ov} = 2.6$ nm, $\rho_{ov} = 3.46\times10^{22}$ atoms cm^{-3}, and $a_{ov} =$ 0.31 nm.[25]

Equivalent surface oxide monolayer calculations: The amount of surface oxide was determined by examining the high-resolution scan of the Si 2p region. Oxidation of silicon surfaces would lead to shifted Si 2p peaks located between 100 and 104 BeV, corresponding to Si^{+}-Si^{4+} oxides in contrast to the bulk Si 2p peak at 99.4 BeV. The bulk

Si $2p_{1/2}$ and Si $2p_{3/2}$ peaks were not resolved (Figure 5a) due to the scan resolution (<0.6 BeV) used in the present work. The surface oxides and bulk silicon 2p peaks were fitted to two peaks, accordingly. The peak areas were then obtained for further oxide monolayer coverage calculation.

Based on the substrate-monolayer model, the thickness of the SiO_x was determined according to the following equation:[25]

$$d_{\mathrm{SiOx}} = \ln[\left(\frac{I_{\mathrm{ov}}}{I_{\mathrm{Si}}}\right)\left(\frac{I^{\mathrm{o}}_{\mathrm{Si}}}{I^{\mathrm{o}}_{\mathrm{ov}}}\right)+1]\lambda_{\mathrm{SiOx}}\mathrm{Sin}\theta \tag{3.3}$$

where $I^{\mathrm{o}}_{\mathrm{Si}} / I^{\mathrm{o}}_{\mathrm{ov}}$ is an instrument normalization factor (1.3 for our instrument), λ_{SiOx} is, as before, the attenuation factor of the overlayer (2.6 nm).[25] The calculated thickness was divided by the thickness of a monolayer of SiO_2, 0.35 nm, to obtain the approximate monolayer coverage.

For very thin oxide monolayers, the following simple method is used to calculate the coverage. Assuming negligible differences in the photoionization cross-sections of surface and bulk Si species ($S_{\mathrm{Si,oxides}} \sim S_{\mathrm{Si,bulk}} = S_{\mathrm{Si}}$), the total observed Si 2p signal per unit surface area is[22]

$$I_{\mathrm{Si,total}} = I_{\mathrm{Si,oxides}} + I_{\mathrm{Si,bulk}} = n_{\mathrm{Si}} S_{\mathrm{Si}} d_{\mathrm{Si}} \mathrm{Sin}\theta \tag{3.4}$$

where n_{Si} is the atomic number density of Si (5.0×10^{22} atoms cm^{-3}), S_{si} is the photoionization cross-section of Si, d_{Si} is the photoelectron penetration depth (1.6 nm), and θ is, as before, the takeoff angle (35°). The measured signal from oxidized silicon species per unit surface area is given by:[22, 25]

$$I_{\mathrm{Si,oxides}} = n_{\mathrm{Si,surf}} \sigma_{si,oxides} S_{\mathrm{Si}} \tag{3.5}$$

where $\sigma_{\mathrm{Si,oxides}}$ is the equivalent monolayer coverage of SiO_x. Then we have

$$\frac{I_{\mathrm{Si,oxides}}}{I_{\mathrm{Si,total}}} = \frac{n_{\mathrm{Si,surf}}\sigma_{si,oxides}S_{\mathrm{Si}}}{n_{\mathrm{Si}}S_{\mathrm{Si}}d_{\mathrm{Si}}\mathrm{Sin}\theta} = \frac{n_{\mathrm{Si,surf}}\sigma_{si,oxides}}{n_{\mathrm{Si}}d_{\mathrm{Si}}\mathrm{Sin}\theta} \tag{3.6}$$

Substituting into eq. (3.6) yields $\sigma_{si,oxides} = 5.88 \times (I_{\mathrm{Si,oxides}} / I_{\mathrm{Si,total}})$.

3.3 XPS and IR analysis

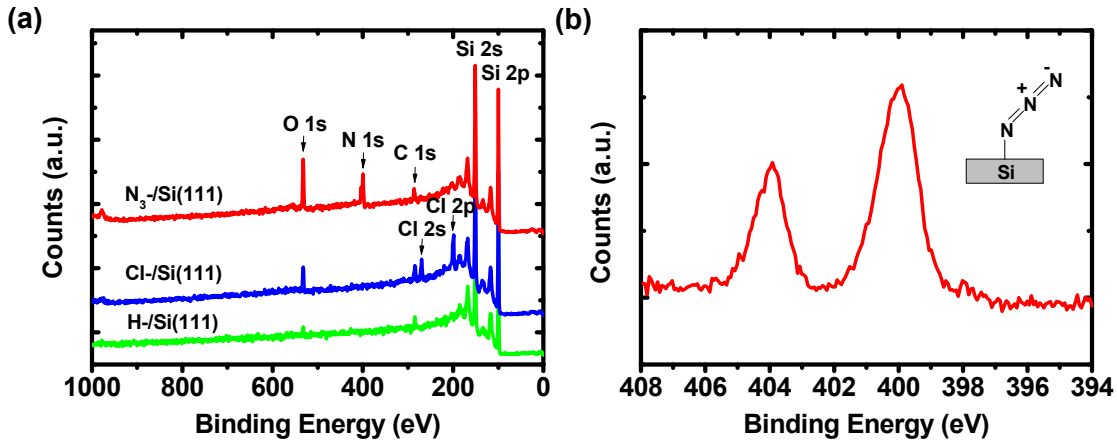

Figure 3.2. XPS analysis of azide-terminated Si(111) surfaces. (a) XPS survey scans following steps of hydrogenation, chlorination and azidation of Si(111) surfaces in Figure 3.1. (b) A high-resolution view of the N (1S) region for N_3^-/Si(111). Inset shows a schematic of the azide-silicon binding configuration. Spectroscopic characterization reveals the surface chemical changes that occur from H-/Si(111) to Cl-/Si(111) to N_3^-/Si(111).

XPS data were collected to follow the steps of the reaction scheme (Figure 3.1) and are summarized in Figure 3.2a. In the azidation step, the striking change is the partial disappearance of Cl (80-90%) and appearance of nitrogen peaks corresponding to the presence of azides. The close-up scan of the N 1s region is also shown in Figure 3.2b. Two peaks are clearly resolved at 400 and 404 eV with an intensity ratio of 2:1, similar to

what is seen for azide groups on gold[27] and graphitic[28] surfaces. These characteristic peaks from azide groups show evidence for the presence of azide on the surface. Additionally, no sodium signal was observed from the azide-modified surfaces. This may rule out the possible physically adsorbed species, which may interfere with the spectrum.

Other than these significant changes, peaks from oxygen and carbon are also observable. For instance, a small amount of C and O was observed on H-terminated Si(111) (Figure 3.2a), corresponding to a 0.2±0.1 and 0.3±0.1 monolayer (ML) respectively. After chlorination, these numbers increased to 0.3±0.1 and 0.7±0.2 respectively. The peak ratio of O 1s relative to Si 2p is similar to that observed in the literature.[22] This may be due to adventitiously adsorbed species, since no SiO_x peak was observed through the above two steps (Figure 3.5). In addition, reactions of methanol and THF have also been studied in detail by Amy and coworkers.[29] Partial methoxylation of the surface may also contribute to this. Following azidation, the carbon peak remains similar to that of Cl-/Si, while O 1s increased to 1.3±0.4 ML for both samples prepared from HMPA and methanol. However, assignment of this to oxides would be not possible since the signal from SiO_x in the Si 2p region (Figure 3.5) was almost close to the noise level. It is likely that more water vapor may be adsorbed to the azidated surface while transferring samples to the XPS chamber, since a ~10° decrease in water contact angle has been observed relative to Cl-/Si.

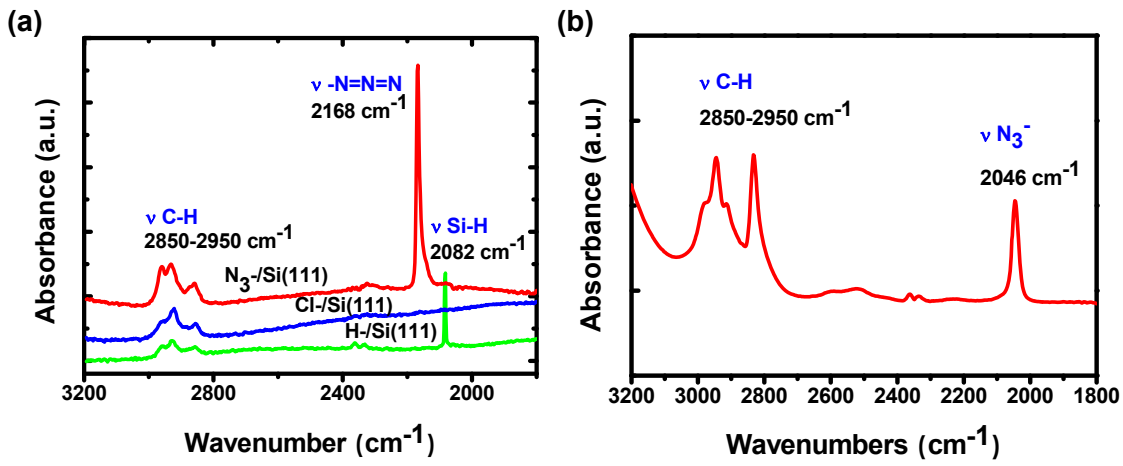

Figure 3.3. ATR-IR data from azide-terminated Si(111) surfaces. (a) IR spectra (referenced to the SiO_2-/Si(111) surfaces) following steps of hydrogenation, chlorination and azidation of silicon surfaces in Figure 3.1. (b) An IR spectrum from sodium azide in a solution of methanol. N_3-/Si(111) surfaces were prepared from the HMPA method. Similar results were also obtained from surfaces prepared from the methanol solution.

The corresponding IR spectra (referenced to SiO_2-/Si(111)) are shown in Figure 3.3a together with that of sodium azide dissolved in methanol. The observation of C-H vibrations in all spectra is due to either adventitiously adsorbed carbon or partial surface methoxylation. The disappearance of the Si-H stretch mode (2082 cm^{-1}) upon chlorination was expected.[24] The most striking feature is the appearance of a unique azide symmetric stretching mode at 2168 cm^{-1}, which is blue-shifted by ~122 and ~63 cm^{-1} with respect to either azides in solution (Figure 3.3b), or organic azides[27, 30] with nitrogen bonded to a carbon atom, respectively. These large frequency shifts suggested the formation of a covalent Si-N bond. The azide symmetric stretch at ~2170 cm^{-1} observed for silyl azide (SiH_3N_3)[31] supports this assignment.

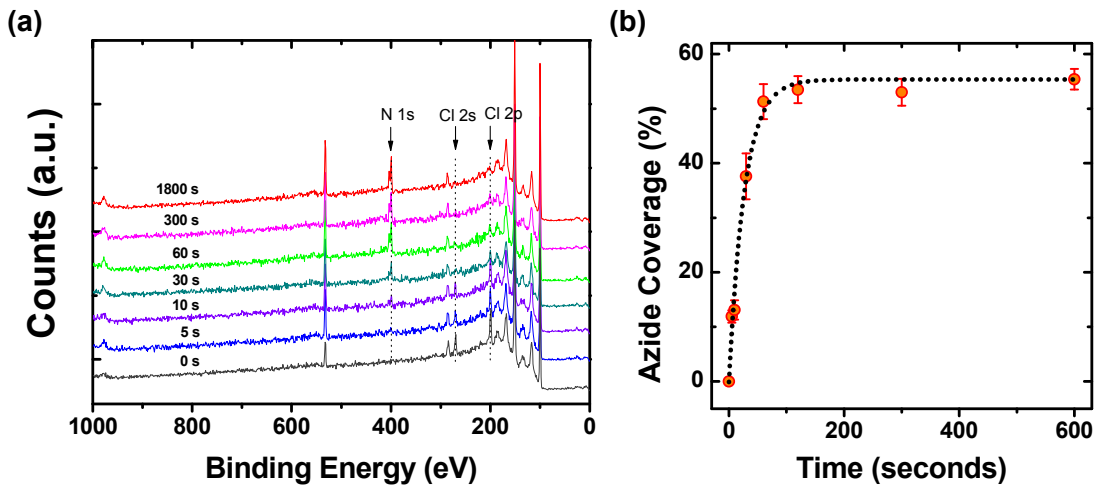

Figure 3.4. Kinetics of azidation of Si(111) surfaces. (a) XPS survey scan of azidated silicon surfaces as a function of reaction time. (b) Plot of surface coverage of azides versus time during the azidation process. The dotted line is a first-order exponential fit of the data from which one can derive a pseudo first-order rate constant of k = 0.037 s^{-1}.

Figure 3.4a shows XPS survey scans of azidated silicon surfaces as a function of reaction time. The opposite trend of the peak intensities of N and Cl elements is clearly observed. By taking the ratio of the normalized, integrated band intensities of N 1s and Si 2p peaks, the coverage of azide on Si(111) was obtained (calculated[25] assuming that 100% coverage means every atop silicon site is capped by an azide group) and plotted as a function of reaction time in Figure 3.4b (circles). For HMPA solvent, the azide coverage reaches about 55%, with a fast, pseudo first-order rate constant of 0.037 s^{-1}. This may be due to the extremely strong solvation ability of cations by HMPA. The corresponding reaction in MeOH was much slower, taking 2-3 hrs to reach a lower level of azide coverage (~25%).

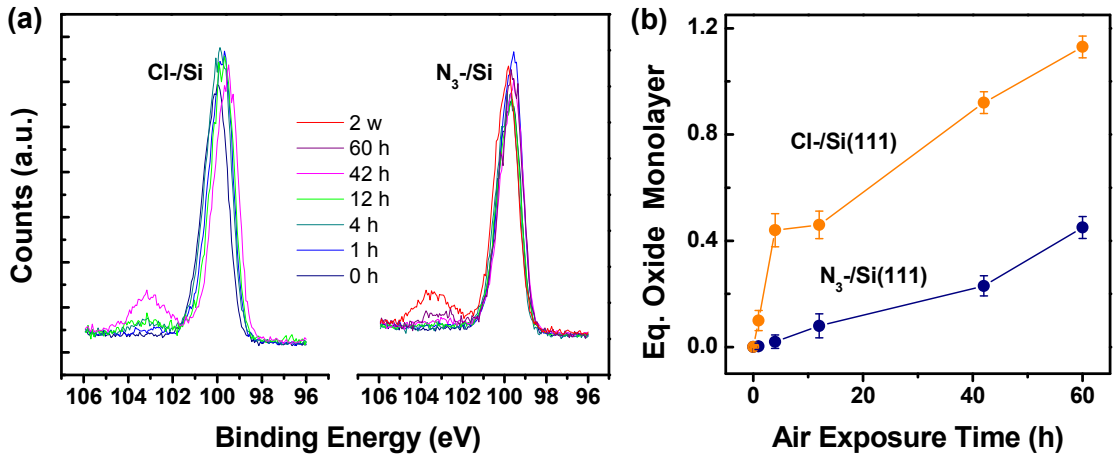

Figure 3.5. Stability of azidated Si(111) surfaces against air oxidation. (a) XPS results for the Si 2p region of azidated silicon surfaces as a function of air exposure time. (b) Plot of equivalent monolayers of SiO_2 formed on the corresponding surfaces in (a) versus time for both N_3-/Si(111) and Cl-/Si(111).

We also utilized XPS to monitor the stability of the N_3-/Si(111) surface in air (relative humidity: ~60%). These data are plotted to show the time-dependent growth of equivalent surface monolayers of SiO_2[22] and are presented in Figure 3.5b. Raw XPS spectral data are in Figure 3.5a, where only the relevant Si 2p region is presented. For freshly prepared Cl-/Si(111) and N_3-/Si(111), signals from silicon oxides at approximately 102-105 BeV are essentially at the noise level. As exposure time increases, signals from this region start to appear, indicating oxide growth on both surfaces. The N_3-/Si(111) surfaces are relatively stable in air compared to chlorinated Si(111), but a full equivalent monolayer of SiO_2 does grow after a 2 week exposure to air. The rapid initial oxidation observed for Cl-/Si(111) was absent for N_3-/Si(111), possibly because the most reactive Cl sites had been replaced with azide. The N_3-/Si(111) is unstable relative to the H_3C-/Si(111) and H_3C-CH_2-/Si(111) surfaces, both of which exhibit higher % coverages, and long-term stability in air.[6, 7]

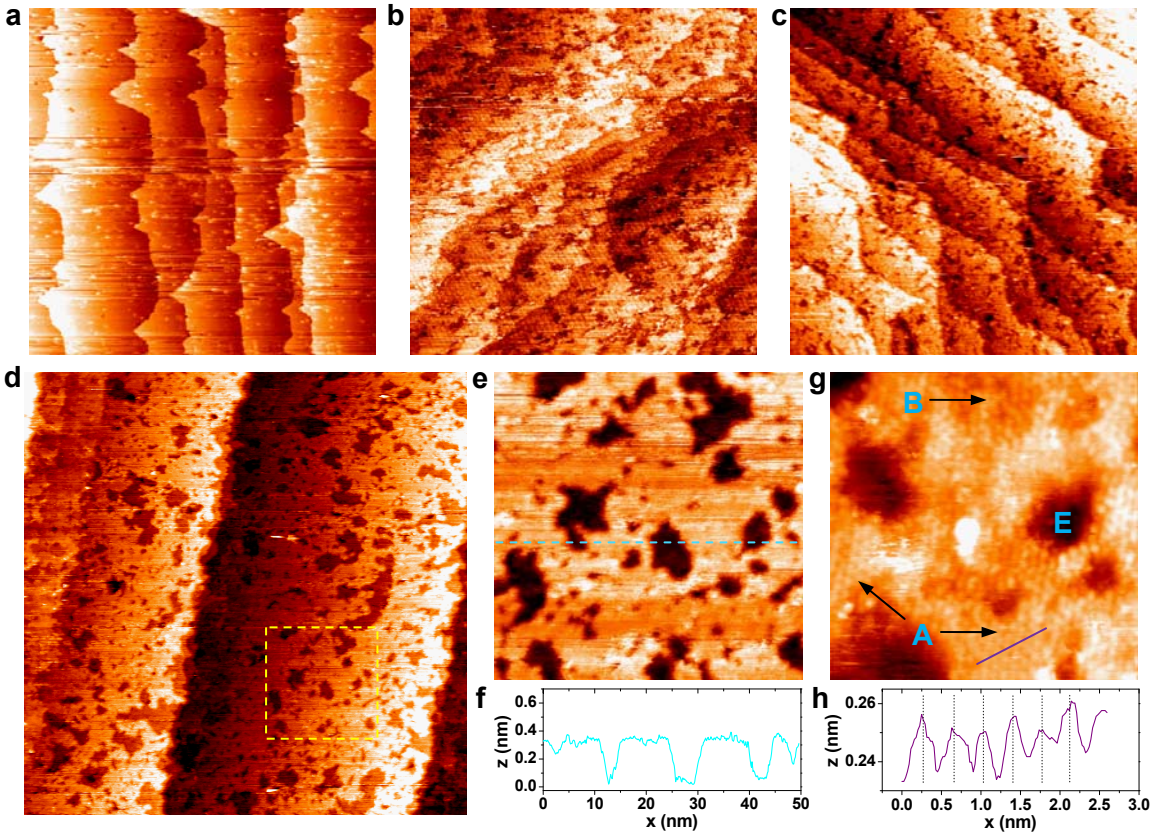

Figure 3.6. Morphology evolutions following the two-step chlorination/azidation process. Constant-current STM images of freshly prepared (a) H-, (b) Cl-, and (c) azide-terminated Si(111) surfaces. (d) Constant-current STM image of another azidated silicon sample prepared from sodium azide in methanol. (e) A close-up of the yellow square in (d). (f) A height profile along the light blue line. (g) A close-up image showing the atoms resolved on the same sample surface as (d). Other than etch pits (dark regions, labeled E), there are also ordered regions (A) and disordered regions (B) coexisting on the image. (h) A height profile along the purple line (left to right) in (g). Dotted lines with a periodicity of 0.38 nm are superimposed on the line profile. Image sizes: 200 nm × 200 nm for (a-d), 50 nm × 50 nm for (e) and 10 nm × 10 nm for (g). Height scales: 1 nm for (a-d) and 0.4 nm for (e)(g).

3.4 STM and STS analysis

The morphology of the azidated surfaces were studied by STM and the images are presented in Figure 3.6c. Figure 3.6d shows another sample with a zoom-in area (yellow box) presented in Figure 3.6e. In these images, brighter colors represent higher regions while darker colors represent lower regions. Both step edges and etch pits were observed. The etch pits are at least one silicon double-layer step lower in height (Figure 3.6f). These observations are similar to that observed from Cl-Si (Figure 3.6b),[32] indicating no significant morphology changes upon azidation. As we have discussed in Chapter 1, these etch pits mainly originate from the chlorination step, since there are significantly fewer etch pits on H-terminated surfaces (Figure 3.6a).

Figure 3.6g displays a constant-current image from the same sample as Figure 3.6d, where atoms (of unknown type) are resolved. Other than the etch pits (labeled E), two types of features are observed on the top layer: ordered (A) and disordered regions (B). Figure 3.6h shows a height profile along the line in the ordered region in Figure 3.6g. Dotted lines with a periodicity of 0.38 nm are also superimposed on the plot. Clearly, the peaks representing atoms are roughly equally spaced in distance with a periodicity of 0.38 nm. This is the characteristic distance between the nearest neighbor silicon atop surface atoms on an unreconstructed Si(111) surface. However, there are also disordered regions (B in Figure 3.6g) where the next neighbor distances are generally not equal to 0.38 nm (height profile not shown here).

To identify the chemical groups on the surface and so as to gain deeper understanding of the surface chemistry, current imaging tunneling spectroscopy (CITS) data are collected (at -1.0V and 77K) from these surfaces (Figure 3.7b), including step

and etch pit edges (red), terrace sites (light blue), and regions of high conductivity (green). The simultaneously collected topographic image is presented in Figure 3.7a.

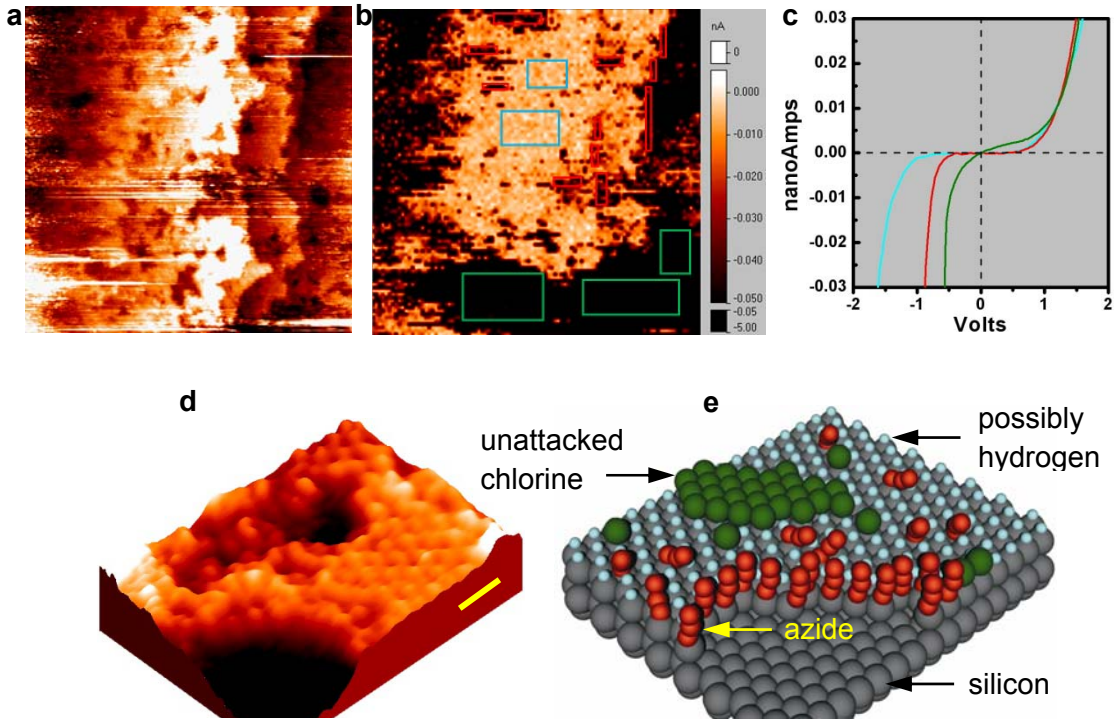

Figure 3.7. Identification of surface chemical groups on azidated Si(111). (a) The topology of the azidated Si(111) surface (at -1.0 V, scale bar: 20 nm). (b) The corresponding CITS image of the same area as (a) together with (c) the averaged STS data (*color-coded*) from various regions of the surface. In this image, *red boxes* encircle step and etch pit edges, *light blue boxes* encircle terrace sites, and *green boxes* encircle regions of high surface conductivity. (d) Constant current STM image of the same Si(111) surface. V_b = 1.85 V, I_t = 0.12 nA, temperature = 77K, scale bar: 1 nm; (e) Graphic illustrating the assigned chemical groups on the azidated Si(111) surface.

Three distinct regions (color-coded on Figures 3.7b-c) were found in terms of yielding distinct I-V tunneling curves, suggesting areas with different chemical origins.

The terrace sites (light blue encircled regions) showed a band gap of about 1.5 V, which is close to that (1.6 V) observed for H-/Si(111),[32] while step and etch pit edges (red) exhibit a gap value of about 0.8 V. The high conductance regions (green) appear similar to that of Cl-/Si(111), namely, nonzero slope or nonzero density of states at zero bias.[32] We thus tentatively assign the red-encircled regions as azide-covered (see the drawing of Figure 3.7e). Figure 3.7d displays a constant-current 3D image from N_3-/Si(111) with low azide coverage (~25%), where atoms are resolved. Upon higher coverage of azide (55%), the three distinct classes of I-V traces are still observed, but are more evenly distributed over the surface (not shown here).[1]

3.5 Conclusion

In this chapter, we have described methods to covalently attach the azide functionality to Si(111) surfaces through a two-step chlorination/azidation process. It is shown to yield different azidation kinetic rates, different final azide coverages, and different surface-area distributions, depending upon the azidation solvent. Similar to the previously reported HC≡C-/Si(111) surface,[23] the N_3-/Si(111) surface should be useful for secondary functionalization through the Cu(I)-catalyzed Huisgen 1,3-dipolar cycloaddition ("click" chemistry).[33] Alternatively, reduction of the N_3-/Si(111) surface using the Staudinger reduction method[34] would be expected to produce an amine-terminated surface for the coupling of carboxylic acid molecules.

3.6 References

1. Cao, P.G., Xu, K. & Heath, J.R. Azidation of silicon(111) surfaces. *J Am Chem Soc* **130**, 14910-14911 (2008).

2. Buriak, J.M. Organometallic chemistry on silicon and germanium surfaces. *Chem Rev* **102**, 1271-1308 (2002).

3. Linford, M.R. & Chidsey, C.E.D. Alkyl monolayers covalently bonded to silicon surfaces. *J Am Chem Soc* **115**, 12631-12632 (1993).

4. Linford, M.R., Fenter, P., Eisenberger, P.M. & Chidsey, C.E.D. Alkyl monolayers on silicon prepared from 1-alkenes and hydrogen-terminated silicon. *J Am Chem Soc* **117**, 3145-3155 (1995).

5. Nemanick, E.J. et al. Chemical and electrical passivation of single-crystal silicon(100) surfaces through a two-step chlorination/alkylation process. *J Phys Chem B* **110**, 14770-14778 (2006).

6. Webb, L.J. et al. High-resolution soft X-ray photoelectron spectroscopic studies and scanning auger microscopy studies of the air oxidation of alkylated silicon(111) surfaces. *J Phys Chem B* **110**, 23450-23459 (2006).

7. Yu, H.B. et al. Scanning tunneling microscopy of ethylated Si(111) surfaces prepared by a chlorination/alkylation process. *J Phys Chem B* **110**, 23898-23903 (2006).

8. Jaeckel, B., Hunger, R., Webb, L.J., Jaegermann, W. & Lewis, N.S. High-resolution synchrotron photoemission studies of the electronic structure and thermal stability of CH3- and C2H5-functionalized Si(111) surfaces. *J Phys Chem C* **111**, 18204-18213 (2007).

9. Haick, H., Hurley, P.T., Hochbaum, A.I., Yang, P.D. & Lewis, N.S. Electrical characteristics and chemical stability of non-oxidized, methyl-terminated silicon nanowires. *J Am Chem Soc* **128**, 8990-8991 (2006).

10. Green, J.E., Wong, S.J. & Heath, J.R. Hall mobility measurements and chemical stability of ultrathin, methylated Si(111)-on-insulator films. *J Phys Chem C* **112**, 5185-5189 (2008).

11. Strother, T., Cai, W., Zhao, X.S., Hamers, R.J. & Smith, L.M. Synthesis and characterization of DNA-modified silicon (111) surfaces. *J Am Chem Soc* **122**, 1205-1209 (2000).

12. Pike, A.R. et al. DNA on silicon devices: On-chip synthesis, hybridization, and charge transfer. *Angew Chem Int Edit* **41**, 615-616 (2002).

13. Linford, M.R. & Chidsey, C.E.D. Surface functionalization of alkyl monolayers by free-radical activation: Gas-phase photochlorination with Cl-2. *Langmuir* **18**, 6217-6221 (2002).

14. Rohde, R.D., Agnew, H.D., Yeo, W.S., Bailey, R.C. & Heath, J.R. A non-oxidative approach toward chemically and electrochemically functionalizing Si(111). *J Am Chem Soc* **128**, 9518-9525 (2006).

15. Fellah, S. et al. Grafting and polymer formation on silicon from unsaturated Grignards: I - Aromatic precursors. *J Phys Chem B* **110**, 1665-1672 (2006).

16. Fellah, S. et al. Grafting and polymer formation on silicon from unsaturated Grignards: II. Aliphatic precursors. *J Phys Chem B* **111**, 1310-1317 (2007).

17. Ciampi, S. et al. Functionalization of acetylene-terminated monolayers on Si(100) surfaces: A click chemistry approach. *Langmuir* **23**, 9320-9329 (2007).

18. Marrani, A.G. et al. Functionalization of Si(100) with ferrocene derivatives via "click" chemistry. *Electrochim Acta* **53**, 3903-3909 (2008).

19. Plass, K.E., Liu, X.L., Brunschwig, B.S. & Lewis, N.S. Passivation and secondary functionalization of allyl-terminated Si(111) surfaces. *Chem Mater* **20**, 2228-2233 (2008).

20. Rivillon, S., Brewer, R.T. & Chabal, Y.J. Water reaction with chlorine-terminated silicon (111) and (100) surfaces. *Appl Phys Lett* **87**, 173118 (2005).

21. Rivillon, S. et al. Chlorination of hydrogen-terminated silicon(111) surfaces. *J Vac Sci Technol A* **23**, 1100-1106 (2005).

22. Webb, L.J. & Lewis, N.S. Comparison of the electrical properties and chemical stability of crystalline silicon(111) surfaces alkylated using Grignard reagents or olefins with Lewis acid catalysts. *J Phys Chem B* **107**, 5404-5412 (2003).

23. Hurley, P.T., Nemanick, E.J., Brunschwig, B.S. & Lewis, N.S. Covalent attachment of acetylene and methylacetylene functionality to Si(111) surfaces: Scaffolds for organic surface functionalization while retaining Si-C passivation of Si(111) surface sites. *J Am Chem Soc* **128**, 9990-9991 (2006).

24. Bansal, A., Li, X.L., Yi, S.I., Weinberg, W.H. & Lewis, N.S. Spectroscopic studies of the modification of crystalline Si(111) surfaces with covalently-attached alkyl chains using a chlorination/alkylation method. *J Phys Chem B* **105**, 10266-10277 (2001).

25. Haber, J.A. & Lewis, N.S. Infrared and X-ray photoelectron spectroscopic studies of the reactions of hydrogen-terminated crystalline Si(111) and Si(100) surfaces with Br-2, I-2, and ferrocenium in alcohol solvents. *J Phys Chem B* **106**, 3639-3656 (2002).

26. Briggs, D. & Seah, M.P. Practical surface analysis, Edn. 2nd. (Wiley; Salle + Sauerländer, Chichester; New York; 1990).

27. Collman, J.P., Devaraj, N.K., Eberspacher, T.P.A. & Chidsey, C.E.D. Mixed azide-terminated monolayers: A platform for modifying electrode surfaces. *Langmuir* **22**, 2457-2464 (2006).

28. Devadoss, A. & Chidsey, C.E.D. Azide-modified graphitic surfaces for covalent attachment of alkyne-terminated molecules by "click" chemistry. *J Am Chem Soc* **129**, 5370-5371 (2007).

29. Amy, S.R. et al. Investigation of the reactions during alkylation of chlorine-terminated silicon (111) surfaces. *J Phys Chem C* **111**, 13053-13061 (2007).

30. Collman, J.P., Devaraj, N.K. & Chidsey, C.E.D. "Clicking" functionality onto electrode surfaces. *Langmuir* **20**, 1051-1053 (2004).

31. Ebsworth, E.A. & Mays, M.J. The preparation and properties of silyl azide. *J Chem Soc*, 3450-3454 (1964).

32. Cao, P.G., Yu, H.B. & Heath, J.R. Scanning tunneling microscopy and spectroscopy of wet-chemically prepared chlorinated Si(111) surfaces. *J Phys Chem B* **110**, 23615-23618 (2006).

33. Devaraj, N.K. & Collman, J.P. Copper catalyzed azide-alkyne cycloadditions on solid surfaces: Applications and future directions. *Qsar Comb Sci* **26**, 1253-1260 (2007).

34. Gololobov, Y.G., Zhmurova, I.N. & Kasukhin, L.F. 60 years of staudinger reaction. *Tetrahedron* **37**, 437-472 (1981).